Applied Catalysis B: Environmental 255 (2019) 117761

Contents lists available at ScienceDirect

Applied Catalysis B: Environmental

journal homepage: www.elsevier.com/locate/apcatb

Three-dimensional network structure assembled by g-C_3N_4 nanorods for improving visible-light photocatalytic performance

Wenjiao Luo[a], Xianjie Chen[a], Zhen Wei[a], Di Liu[b], Wenqing Yao[a], Yongfa Zhu[a,*]

[a] Department of Chemistry, Tsinghua University, Beijing, 100084, PR China
[b] School of Chemical & Environmental Engineering, China University of Mining & Technology, Beijing, 100083, PR China

ARTICLE INFO

Keywords:
Three-dimensional network structure
Graphitic carbon nitride
Photocatalyst
Nanostructure design
Hydrogen evolution

ABSTRACT

Bulk g-C_3N_4 has suffered from its low specific surface area and high recombination of photogenerated electron-hole pairs. Herein, three-dimensional network structure g-C_3N_4 assembled by nanorods (3D g-C_3N_4 NR) was successfully fabricated via a chemical tailoring route. The as-prepared 3D g-C_3N_4 NR exhibits lager specific surface areas (6.7 times of bulk g-C_3N_4) and faster charge carrier transfer kinetics. Hence, the visible-light photocatalytic activities for degradation of phenol and hydrogen evolution over 3D g-C_3N_4 NR are evidently enhanced, 4.3 and 5.9 times as high as that of bulk g-C_3N_4, respectively. Briefly, this work throws light on structural tuning of carbon nitride polymer photocatalysts for improved solar energy capture and conversion.

1. Introduction

Graphitic carbon nitride (g-C_3N_4) polymer, an appealing kind of photocatalyst for solving energy shortage and environmental pollution, has attracted extensive attention which benefits from its being metal-free, earth-abundance nature, nontoxicity, chemical stability, and visible-light activity [1–3]. Unfortunately, the photocatalytic efficiency of the usual bulk g-C_3N_4 prepared by direct thermal polymerization of cyanamide precursor is still far from satisfaction. It is largely owing to the low specific surface area and high recombination rate of photo-generated electron-hole pairs in bulk g-C_3N_4 [4–6]. To overcome these limitations and thus improve the photocatalytic activity of g-C_3N_4, great efforts have been devoted to the chemical structure modulation and nanostructure design, including copolymerizing with conjugated molecules [7,8], morphology control [9–13], doping with heteroatom [14–17], and compounding with other semiconductors [18–21] etc. Especially, nanostructure design could both increase the specific surface area and facilitate the photogenerated charge carrier transfer, which is able to significantly improve the photocatalytic activity of g-C_3N_4.

Recently, three-dimensional (3D) network structure photocatalysts assembled by low-dimensional nano-units have drawn increasing research interest in energy conversion and environmental remediation. The unique structure not only combines the large specific surface area and fast charge carrier transfer kinetics of low-dimensional nano-units but also maximizes the utilization of incident photons via the multi-reflection within the interconnected network structure [22–26]. Furthermore, 3D network structure would be capable of preventing low-dimensional nano-units from agglomerating. Lately, Zhang's group hydrolyzed bulk g-C_3N_4 in NaOH solution and gained highly dispersible g-C_3N_4 nanofibers with plenty of active groups on surfaces, which could transform into a 3D network g-C_3N_4 hydrogel using CO_2 as a trigger, and the 3D network hydrogel exhibited a competitive absorbing capacity [27]. It was also reported that Wang's group synthesized 3D g-C_3N_4 aerogels consisting of low-dimensional g-C_3N_4 nanoparticle units through an aqueous sol-gel strategy, which possessed high specific surface area and showed excellent photocatalytic activity for hydrogen evolution and H_2O_2 production [28]. Therefore, fabricating 3D network structure by assembling low-dimensional nano-units is an effective and practical route to improve the photocatalytic efficiency of g-C_3N_4.

Herein, a facile strategy of chemical tailoring, self-assembling and repolymerizing the heptazine units, using bulk g-C_3N_4 as the starting material, is developed to fabricate 3D network structure g-C_3N_4 assembled by nanorods (3D g-C_3N_4 NR). 3D g-C_3N_4 NR possesses larger specific surface area and faster charge carrier transfer kinetics, thus it shows significantly enhanced photocatalytic activity for degradation of phenol and hydrogen evolution. Briefly, this work throws light on structural tuning of carbon nitride polymer photocatalysts for improved solar energy capture and conversion.

* Corresponding author.
E-mail address: zhuyf@tsinghua.edu.cn (Y. Zhu).

https://doi.org/10.1016/j.apcatb.2019.117761
Received 27 March 2019; Received in revised form 9 May 2019; Accepted 17 May 2019
Available online 19 May 2019

2. Experimental section

2.1. Sample synthesis

2.1.1. Synthesis of bulk g-C_3N_4

10 g dicyandiamide was placed into a crucible with a cover, transferred into a muffle furnace, and heated at 550 °C for 4 h with a heating rate of 2.3 °C min^{-1}. The sample was collected and ground thoroughly after naturally cooling to room temperature.

2.1.2. Synthesis of g-C_3N_4 solution

2 g bulk g-C_3N_4 was dispersed into 120 mL nitric acid (65 wt.%) and sealed. Then the mixture was heated at 80 °C in a water bath for 3 h after 30 min sonication. The g-C_3N_4 solution was obtained after centrifugalizing at a speed of 5000 r min^{-1}.

2.1.3. Synthesis of 3D g-C_3N_4 NR

75 mL 10 mol L^{-1} KOH solution was poured into a beaker and 30 mL g-C_3N_4 solution was added dropwise under stirring. The solution turned to be a light white suspension when pH was close to neutral with the regulation by 5 mol L^{-1} nitric acid and followed by adding nitric acid until pH got to 5. Precursor was collected by filtering, washing to neutral with a large amount of de-ionized water, and freeze-drying. Finally, 3D g-C_3N_4 NR was obtained after heating the precursor at 500 °C for 4 h with a heating rate of 2.3 °C min^{-1} under N_2 protection.

2.2. Characterization

The morphologies and structures of synthesized samples were captured by the field emission scanning electron microscopy (FE-SEM, Hitachi SU-8010) at an accelerating voltage of 5 kV and transmission electron microscope (TEM, Hitachi HT7700) at 100 kV. X-ray powder diffraction (XRD) was characterized at 40 kV and 200 mA by a Rigaku D/max-2400 X-ray diffractometer with Cu K 1 (λ = 0.15418 nm) radiation to investigate phase structure. Fourier transform infrared (FT-IR) experiment was recorded on a Bruker V70 spectrometer, equipped with attenuated total reflectance (ATR). UV–vis diffuse reflectance spectra (DRS) were performed on a Hitachi U-3010 spectrophotometer using $BaSO_4$ as the reflectance standard. X-ray photoelectron spectra (XPS) experiments were carried out on a PHI Quantera SXM spectrometer with Al K_α radiation. Steady-state photoluminescence (PL) spectra were performed by a Perkin-Elmer LS55 spectrophotometer with an excitation wavelength of 370 nm. Time-resolved photoluminescence spectra were measured on an Edinburgh FLSP920 fluorescence spectrometer. The solid-state ^{13}C nuclear magnetic resonance (NMR) spectra were collected on a JEOL JNM-ECZ600R spectrometer with the probe diameter of 3.2 mm, 12 kHz rotating speed and 3 s relaxation time.

2.3. Photocatalytic degradation evaluation

The photocatalytic performances were measured on an XPA-7 photochemical reactor (Xujiang Electromechanical Plant, Nanjing, China) using phenol as the probe molecule. Visible light was obtained from a 500 W Xenon lamp with a 420 nm cutoff filter. In a typical photocatalytic experience, 10 mg photocatalyst was placed in a quartz tube and dispersed with 50 mL 5 ppm phenol solution. The mixture was sonicated for 10 min for sufficient dispersion. The suspension was magnetically stirred for 1 h to achieve absorption-desorption equilibrium. 2 mL liquid was sampled every 1.5 h. Particles were removed by centrifugation. The concentration of phenol was detected by a high performance liquid chromatography (HPLC) with an ultraviolet absorbance detector operated at 270 nm and a Venusil XBP-C18 column (Agela Technologies Inc.) after ultrafiltration through millipore filter membranes of 0.22 mm. Mobile phase consisted of water and methanol (V_{water}: $V_{methanol}$ = 45: 55) with the flow rate of 1 mL min^{-1} and elution time was 5 min. The degradation processes of phenol for all samples were fitted to pseudo-first-order kinetics.

2.4. Photocatalytic H_2 evaluation

The photocatalytic activities for hydrogen evolution of as-prepared samples were evaluated by using a Perfect Light agitated reactor (Labsolar-6A, PerfectLight). Visible light was obtained from a 300 W Xenon lamp with a 420 nm cutoff filter. 10 mg photocatalyst was added into 100 mL solution (90 mL deionized water and 10 mL triethanolamine as sacrificial agent). 1 wt.% Pt as co-catalysts were loaded on the photocatalysts by in situ photo-deposition method using H_2PtCl_6. Before light irradiation, the suspensions were ultrasonically dispersed -in the dark for 30 min to achieve absorption-desorption equilibrium. At given time intervals (30 min), a certain amount of produced gas was measured by an online gas chromatograph (GC-2002 N/TFF) equipped with a thermal conductive detector (TCD) and a 13X-5 Å molecular sieve column, using Ar as the carrier gas. Product gases were calibrated with standard H_2 gas and their identities were determined according to the retention time.

3. Results and discussion

3.1. 3D network structure g-C_3N_4 assembled by nanorods

3D g-C_3N_4 NR could be controllably synthesized via a facile route, as shown in Fig. 1a, containing chemical tailoring, self-assembling and repolymerizing the heptazine units, using bulk g-C_3N_4 as the starting material. Firstly, bulk g-C_3N_4 was tailored into little pieces with a small amount of heptazine ring repeating units with -NH_x and −OH groups by treating with hot concentrated nitric acid. The van der Waals force between C–N layers in g-C_3N_4 could be effectively destroyed under this condition of strong acidity and high temperature [29–31]. Meanwhile, the structural hydrogen bonding between melon units in bulk g-C_3N_4 could be broken by the strong oxidation of nitric acid [30]. The FT-IR spectrum of the precursor (Fig. S1a) suggests the existence of heptazine ring and −NH_x/−OH groups in these pieces. Thus, when pH was close to neutral, these pieces could self-assemble into the nanorod-like precursor via hydrogen bonds like N−H···O, N−H···N in layers and π-π conjugation between layers. Since the number of heptazine rings in small pieces may vary, precursor exhibits poor in-plane repeatability but strong interlayer stacking which is revealed by the result of XRD in Fig. S1b.

Meanwhile, these nanorods precursor intertwined to form a 3D network structure. And it can be clearly seen from Fig. 1c that the 3D network structure precursor is assembled by a large number of nanorods with diameter below 50 nm. Finally, 3D g-C_3N_4 NR was obtained by further thermal repolymerizing of precursor. Compared with its precursor, 3D g-C_3N_4 NR substantially maintained the nanorod-like morphology and the diameter, but the length slightly shortened (Fig. 1d). As shown in Fig. 1e, the cross-linking occurred between adjacent nanorods during the thermal polycondensation, resulting in a more compact three-dimensional network structure significantly different from the micron block structure of bulk g-C_3N_4.

Benefiting from its three-dimensional network structure assembled by nanorods, 3D g-C_3N_4 NR presents a pore structure as well as quite large specific surface area, up to 60.95 $m^2 g^{-1}$, which is 7.4 times higher than that of bulk g-C_3N_4 (8.22 $m^2 g^{-1}$). It is worth mentioning that the pore structure in 3D network could facilitate the rapid transfer of reactants and products during photocatalytic reaction. In XRD patterns (Fig. 2b), two distinct diffraction peaks in bulk g-C_3N_4 located at 12.84° and 27.36° are indexed to the (100) and (002) peaks for graphitic materials, corresponding to in-plane structural packing motif and interlayer stacking, respectively [11,32]. Compared with bulk g-C_3N_4, the intensity of (002) peak in 3D g- C_3N_4 NR significantly decreases while (100) peak is almost unrecognizable, which is due to the reduced

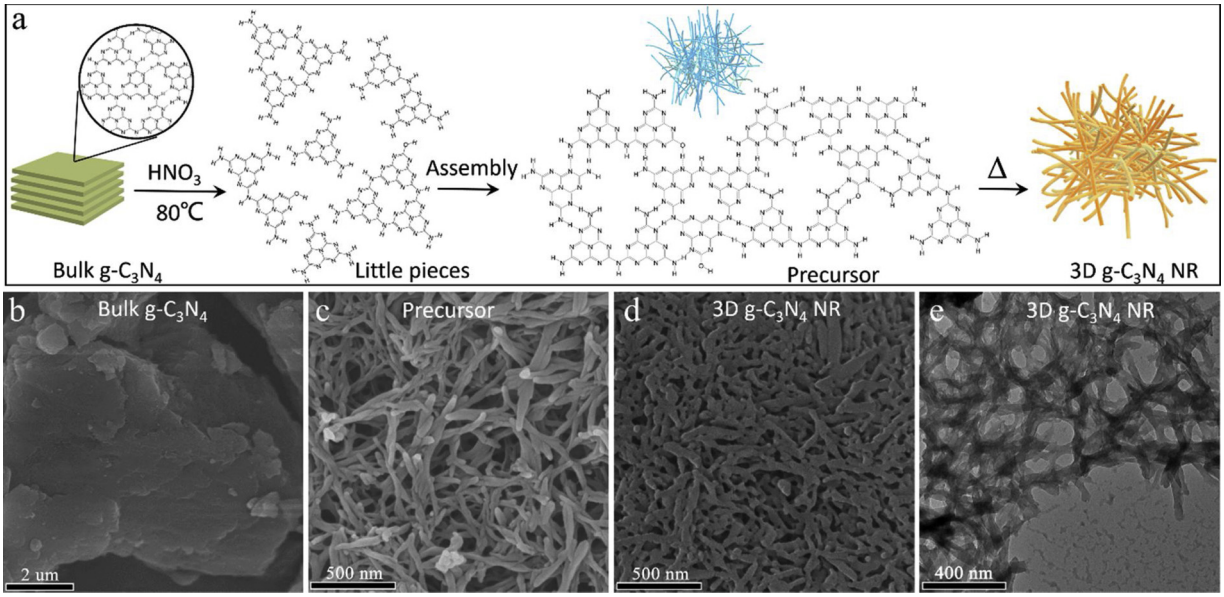

Fig. 1. Schematic illustration of the synthetic route for 3D g-C_3N_4 NR (a), SEM images of bulk g-C_3N_4 (b), precursor (c) and 3D g-C_3N_4 NR (d), TEM image of 3D g-C_3N_4 NR (e).

stacking of repeat units along the plane direction in low-dimensional nanorods. In FT-IR spectra (Fig. 2c), all the bands assigned to typical CN polymer are visible in both bulk g-C_3N_4 and 3D g-C_3N_4 NR [33]. The prominent absorption at 806.2 cm^{-1} is contributed to out-of-plane bending vibration of tri-s-triazine. The strong bands at 1627.9, 1564.2, 1456.2 and 1406.1 cm^{-1} represent the typical stretching vibration of heptazine ring. The peaks at 1317.3 and 1236.3 cm^{-1} are in agreement with stretching vibration of C—N(—C) with complete polycondensation or C—NH—C with partial polycondensation [34]. The broad weak band between 3000 and 3300 cm^{-1} indicates the presence of NH and/or NH_2 groups. Moreover, the solid-state ^{13}C CP-MAS NMR spectrum of 3D g-C_3N_4 NR (Fig. S2) presents two strong signals at 156.9 and 164.3 ppm, corresponding to the chemical shifts of C_3N (1) and C_2N-NH_x (2), respectively [6], which further confirms the existence of tri-s-triazine units. Additionally, XPS spectra were recorded to reveal more details about compositions and chemical states of the as-prepared samples. As seen in Fig. 2d, bulk g-C_3N_4 and 3D g-C_3N_4 NR have similar spectra. In C 1s spectrum, the peak at 288.4 eV originates from N=C—N structure, and the peak at 284.8 eV is caused by contaminated carbon [35,36]. In N 1s spectra, the existence of C—N=C structure is demonstrated by the

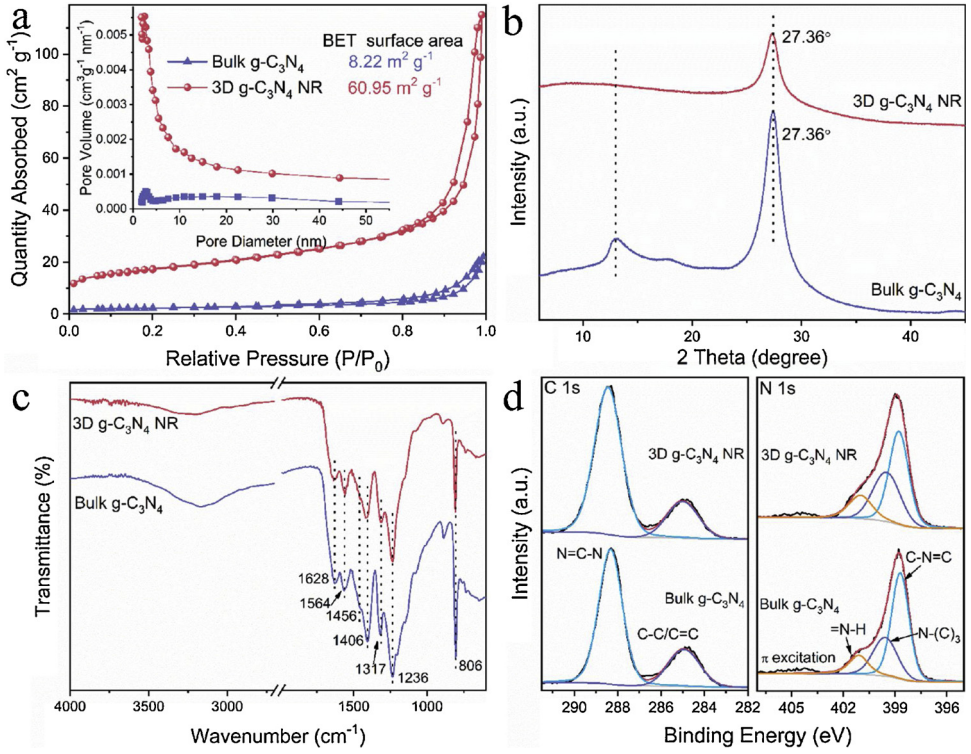

Fig. 2. Nitrogen isothermal adsorption-desorption curves (Pore volume distribution inset) (a), XRD patterns (b), FT-IR spectra (c), XPS spectra of C1 s (left) and N1 s (right) (d) of bulk g-C_3N_4 and 3D g-C_3N_4 NR.

binding energy at 398.86 eV. And the peak at 400.0 eV is the signal of N connecting three C atoms at the center and bridge of heptazine ring (N—C_3), whereas the contribution at 401.44 eV is caused by amino group (C—NH). Besides, the peak at 404.55 eV is mainly attributed to the charging effect and the excitation of π electrons [37,38]. Therefore, compared with bulk g-C_3N_4, 3D g-C_3N_4 NR hasn't been changed in the chemical composition, but only changed in the morphology and structure.

3.2. Faster charge carriers separation over 3D g-C_3N_4 NR

The low-dimensional nanorod-like structure of g-C_3N_4 photocatalysts has been proved to effectively suppress the recombination of photogenerated electron-hole pairs [39–41]. It is well known that separation efficiency of photogenerated electron-hole pairs is one of the determining steps in photocatalytic reaction. Thus, fluorescence spectra and photoelectrochemical experiments were performed to investigate the separation efficiency of photogenerated charge carriers over 3D g-C_3N_4 NR. The intensity of PL spectrum is a direct proof for electron-hole recombination rate, while the more efficient charge carrier separation results in the lower intensity. In steady-state PL emission spectra, as shown in Fig. 3a, the feature peak near 453 nm corresponds to the intrinsic π-π* electronic transition [42,43]. The intensity in 3D g-C_3N_4 NR decreases sharply, only 3.84% of bulk g-C_3N_4, which suggests that the recombination of photogenerated electron-hole pairs in 3D g-C_3N_4 NR is effectively suppressed. It is further verified by the results of time-resolved fluorescence decay curves (Fig. 3b). The lifetime is contributed by three different processes: non-radiative process (τ_1), radiative process (τ_2) and energy transfer process (τ_3). The radiative process (τ_2) is directly related to the recombination of photogenerated electron-hole pairs, [44] and it comes to 6.97, 5.55 ns for 3D g-C_3N_4 NR and bulk g-C_3N_4, respectively. The longer lifetime in radiative process suggests that 3D g-C_3N_4 NR exhibits more efficient separation of electrons and holes [45]. Furthermore, the improved changer carrier mobility of 3D g-C_3N_4 NR could be very classically supported by the increased photocurrent (Fig. 3c) and the decreased charge transfer resistance (Rsc) estimated via fitting the hemicycle radius on electrochemical impedance spectroscopy (EIS) in Fig. 3d, which determined to 657.7, 1812.0 kΩ for 3D g-C_3N_4 NR and bulk g-C_3N_4, respectively. The faster charge carriers separation and mobility are largely owing to the reduced carriers migration distance to photocatalyst surface.

Besides, UV–vis diffuse reflectance spectra of as-prepared samples in Fig. S4a feature typical semiconductor-like absorptions. Compared to bulk g-C_3N_4, 3D g-C_3N_4 NR shows stronger absorption intensities under both ultraviolet and visible light, which is favorable for improving photocatalytic activity by the enhanced light harvest. It is believed that the enhanced optical absorption of 3D g-C_3N_4 NR mainly results from the multiple reflections of incident light in the three-dimensional network structure assembled by nanorods [46–48]. The energy level is calculated by combining the results of DRS and Mott-Schottky curve, and the schematic band structure diagrams are given in Fig. S4d. 3D g-C_3N_4 NR possessing the deeper valence band position is able to produce photogenerated holes with stronger oxidation capability, thus obtains better photocatalytic activity and higher mineralization capacity.

3.3. Highly efficient and stable photocatalytic performance

The enhanced specific surface area of 3D g-C_3N_4 NR, originating from its unique three-dimensional network structure assembled by nanorods, could significantly increase its adsorption capacity and the number of active sites, which is favor of better photocatalytic performance. Fig. S5 shows the comparison of adsorption capacity for MB over bulk g-C_3N_4 and 3D g-C_3N_4 NR. The adsorption capacity of 3D g-C_3N_4 NR for MB is 17.71 mg g^{-1}, 6.7 times higher than that of bulk g-C_3N_4 (2.64 mg g^{-1}). Considering that MB is a kind of cationic dye, the more positive Zeta potential of 3D g-C_3N_4 NR (3D g-C_3N_4 NR: -28.86 mV, bulk g-C_3N_4: -52.92 mV) fully indicates that the higher adsorption of 3D g-C_3N_4 NR originates from the improvement of specific surface area rather than the change of surface charge.

It is reasonable to anticipate that 3D g-C_3N_4 NR is a promising kind of photocatalyst due to the combination of the advantage of three-dimensional network structure and the faster charge carrier transfer

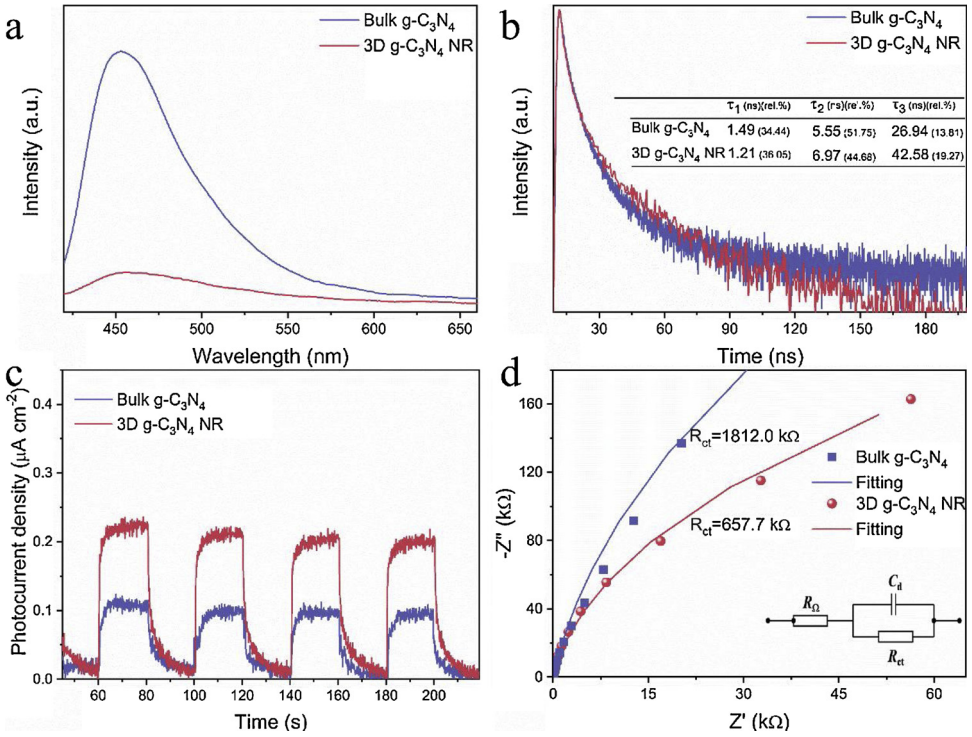

Fig. 3. Steady-state PL emission spectra (a), time-resolved transient PL decay spectra (b), transient photocurrent density (c) and electrochemical impedance spectra (the equivalent circuit impedance model inset) of bulk g-C_3N_4 and 3D g- C_3N_4 NR.

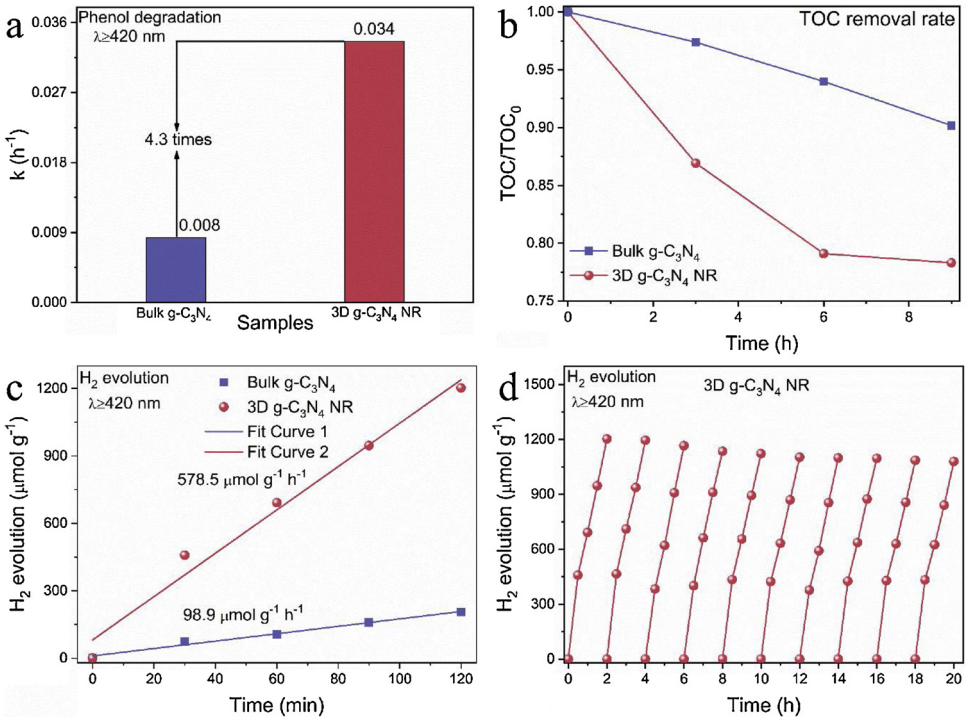

Fig. 4. Photocatalytic degradation for phenol (a), total organic carbon (TOC) removal rate for phenol (b), photocatalytic H_2 evolution (c) of 3D g-C_3N_4 NR and bulk g-C_3N_4. The repeated cycle H_2 evolution of 3D g-C_3N_4 NR (d).

kinetics. In view of this, the photocatalytic performance of 3D g-C_3N_4 NR was evaluated by photocatalytic degradation of phenol and hydrogen evolution under visible light (> 420 nm) irradiation. As shown in Fig. 4a, the photocatalytic degradation activity for phenol over 3D g-C_3N_4 NR is notably improved, while the reaction rate constant *k* reaches 0.034 h^{-1}, 4.3 times as high as that of bulk g-C_3N_4 (0.008 h^{-1}). Besides, 3D g-C_3N_4 NR also exhibits better mineralization ability (Fig. 4b). Its TOC removal rate for phenol could reach 21.7% in 9 h (only 9.8% for bulk g-C_3N_4), which is consistent with the result from the band structure of 3D g-C_3N_4 NR. The hydrogen evolution rates of as-prepared samples are compared in Fig. 4c. 3D g-C_3N_4 NR shows significantly enhanced hydrogen evolution activity with evolution rate of 578.5 μmol g^{-1} h^{-1}, approximately 5.8 times faster than that of bulk g-C_3N_4 (98.9 μmol g^{-1} h^{-1}). In addition, no obvious deactivation emerges over 3D g-C_3N_4 NR during the continuous 10 round experiments under the same reaction conditions (Fig. 4d), suggesting the good stability of 3D g-C_3N_4 NR. It is worth mentioning that the precursor of 3D g-C_3N_4 NR has no photocatalytic activity under visible light irradiation (Fig. S8) due to its low degree of polymerization. Above all, the significant enhanced photocatalytic activity of 3D g-C_3N_4 NR compared to bulk g-C_3N_4 could be attributed to the following reasons: 1) nanorod units greatly reduce the carrier migration distance to photocatalyst surface and accelerate the charge carrier transfer kinetics; 2) three-dimensional network structure exposes more reaction active sites, provides convenient mass transfer channels and then promotes the reaction on the surface of photocatalyst.

4. Conclusion

The as-prepared 3D g-C_3N_4 NR shows significantly enhanced photocatalytic activities for degradation of phenol and hydrogen evolution, approximately 4.3 and 5.9 times higher than that of bulk g-C_3N_4, which is attributed to its nanorod units accelerating the charge carrier transfer kinetics and its 3D network structure affording more surface reaction sites. The superior photocatalytic performance of 3D g-C_3N_4 NR proves that constructing three-dimensional structure assembled by nanorods could effectively address the limitations of bulk g-C_3N_4 suffering from its low specific surface area and high recombination of photogenerated electron-hole pairs. It is believed that this work throws light on structural tuning of carbon nitride polymer photocatalysts for improved solar energy capture and conversion.

Conflict of interest

The authors declare no conflict of interest.

Acknowledgments

This work was financially supported by the National Natural Science Foundation of China (grant numbers21761142017, 21673126, 21621003, and21437003) and the Collaborative Innovation Center for Regional Environmental Quality.

Appendix A. Supplementary data

Supplementary material related to this article can be found, in the online version, at doi:https://doi.org/10.1016/j.apcatb.2019.117761.

References

[1] S. Cao, J. Low, J. Yu, M. Jaroniec, Polymeric photocatalysts based on graphitic carbon nitride, Adv. Mater. 27 (2015) 2150–2176.
[2] Y. Jinhui, W. Donge, H. Hongxian, L. Can, Roles of cocatalysts in photocatalysis and photoelectrocatalysis, Acc. Chem. Res. 46 (2013) 1900–1909.
[3] K. Maeda, K. Teramura, D. Lu, T. Takata, N. Saito, Y. Inoue, K. Domen, Photocatalyst releasing hydrogen from water, Nature 440 (2006) 295.
[4] W.J. Ong, L.L. Tan, Y.H. Ng, S.T. Yong, S.P. Chai, Graphitic carbon nitride (g-C_3N_4)-Based photocatalysts for artificial photosynthesis and environmental remediation: are we a step closer to achieving sustainability? Chem. Rev. 116 (2016) 7159–7329.
[5] W. Jiang, W. Luo, J. Wang, Z. Mo, Y. Zhu, Enhancement of catalytic activity and oxidative ability for graphitic carbon nitride, J. Photochem. Photobiol. C Photochem. Rev. 28 (2016) 87–115.
[6] X. Wang, K. Maeda, A. Thomas, K. Takanabe, G. Xin, J.M. Carlsson, K. Domen, M. Antonietti, A metal-free polymeric photocatalyst for hydrogen production from water under visible light, Nat. Mater. 8 (2009) 76–80.
[7] X. Bai, C. Sun, S. Wu, Y. Zhu, Enhancement of photocatalytic performance via a

P3HT-g-C3N4 heterojunction, J. Mater. Chem. A Mater. Energy Sustain. 3 (2015) 2741–2747.
[8] T. Jordan, N. Fechler, J. Xu, T.J.K. Brenner, M. Antonietti, M. Shalom, "Caffeine doping" of Carbon/Nitrogen-Based organic catalysts: caffeine as a supramolecular edge modifier for the synthesis of photoactive carbon nitride tubes, ChemCatChem 7 (2015) 2826–2830.
[9] Y.S. Jun, J. Park, S.U. Lee, A. Thomas, W.H. Hong, G.D. Stucky, Three-dimensional macroscopic assemblies of low-dimensional carbon nitrides for enhanced hydrogen evolution, Angew. Chem. Int. Ed. Engl. 52 (2013) 11083–11087.
[10] N. Ping, L. Zhang, L. Gang, Hi. Cheng, Graphene-like carbon nitride nanosheets for improved photocatalytic activities, Adv. Funct. Mater. 22 (2012) 4763–4770.
[11] Y. Shubin, G. Yongji, Z. Jinshui, Z. Liang, M. Lulu, F. Zheyu, V. Robert, W. Xinchen, P.M. Ajayan, Exfoliated graphitic carbon nitride nanosheets as efficient catalysts for hydrogen evolution under visible light, Adv. Mater. 25 (2013) 2452–2456.
[12] I. Yohei, C. Laurent, A. Markus, S. Menny, Morphology control and photocatalysis enhancement by the one-pot synthesis of carbon nitride from preorganized hydrogen-bonded supramolecular precursors, Langmuir 30 (2014) 447–451.
[13] J. Zhang, F. Guo, X. Wang, An optimized and general synthetic strategy for fabrication of polymeric carbon nitride nanoarchitectures, Adv. Funct. Mater. 23 (2013) 3008–3014.
[14] L. Gang, N. Ping, S. Chenghua, S.C. Smith, C. Zhigang, L.G. Qing Max, C. Hui-Ming, Unique electronic structure induced high photoreactivity of sulfur-doped graphitic C_3N_4, J. Am. Chem. Soc. 132 (2010) 11642–11648.
[15] Z. Guigang, Z. Mingwen, Y. Xinxin, Q. Xiaoqing, L. Sen, W. Xinchen, Iodine modified carbon nitride semiconductors as visible light photocatalysts for hydrogen evolution, Adv. Mater. 26 (2014) 805–809.
[16] X. Wang, X. Chen, A. Thomas, X. Fu, M. Antonietti, Metal-containing carbon nitride compounds: a new functional organic-metal hybrid material, Adv. Mater. 21 (2010) 1609–1612.
[17] W. Yong, D. Yan, M. Antonietti, H.R. Li, X.F. Chen, X.C. Wang, Excellent visible-light photocatalysis of fluorinated polymeric carbon nitride solids, Chem. Mater. 22 (2010) 5119–5121.
[18] S. Xu, H. Yun, M. Zheng, C. Wei, Solvent-free in situ synthesis of g-C_3N_4/{001}TiO_2 composite with enhanced UV- and visible-light photocatalytic activity for NO oxidation, Appl. Catal. B-Environ. 182 (2016) 587–597.
[19] P. Chen, P. Xing, Z. Chen, X. Hu, H. Lin, L. Zhao, Y. He, In-situ synthesis of $AgNbO_3$/g-C_3N_4 photocatalyst via microwave heating method for efficiently photocatalytic H_2 generation, J. Colloid. Interface Sci. 534 (2019) 163–171.
[20] Y. He, Y. Wang, L. Zhang, B. Teng, M. Fan, High-efficiency conversion of CO_2 to fuel over ZnO/g-C_3N_4 photocatalyst, Appl. Catal. B-Environ. 168 (2015) 1–8.
[21] T. Li, L. Zhao, Y. He, J. Cai, M. Luo, J. Lin, Synthesis of g-C_3N_4/$SmVO_4$ composite photocatalyst with improved visible light photocatalytic activities in RhB degradation, Appl. Catal. B-Environ. 129 (2013) 255–263.
[22] X. Chen, R. Shi, Q. Chen, Z. Zhang, W. Jiang, Y. Zhu, T. Zhang, Three-dimensional porous g-C_3N_4 for highly efficient photocatalytic overall water splitting, Nano Energy 59 (2019) 644–650.
[23] W. Jiang, Y. Zhu, G. Zhu, Z. Zhang, X. Chen, W. Yao, Three-dimensional photocatalysts with a network structure, J. Mater. Chem. A Mater. Energy Sustain. 5 (2017) 5661–5679.
[24] X. Chen, Q. Chen, W. Jiang, Z. Wei, Y. Zhu, Separation-free TiO_2-graphene hydrogel with 3D network structure for efficient photoelectrocatalytic mineralization, Appl. Catal. B-Environ. 211 (2017) 106–113.
[25] X. Li, J. Yu, M. Jaroniec, Hierarchical photocatalysts, Chem. Soc. Rev. 45 (2016) 2603–2636.
[26] W. Jiang, Q. Ruan, J. Xie, X. Chen, Y. Zhu, J. Tang, Oxygen-doped carbon nitride aerogel: a self-supported photocatalyst for solar-to-chemical energy conversion, Appl. Catal. B-Environ. 236 (2018) 428–435.
[27] Y. Zhang, Z. Zhou, Y. Shen, Q. Zhou, J. Wang, A. Liu, S. Liu, Y. Zhang, Reversible assembly of graphitic carbon nitride 3D network for highly selective dyes absorption and regeneration, ACS Nano 10 (2016) 9036.
[28] H. Ou, P. Yang, L. Lin, M. Anpo, X. Wang, Carbon nitride aerogels for the photoredox conversion of water, Angew. Chem. Int. Ed. Engl. 129 (2017) 10905–10910.
[29] X. Du, G. Zou, Z. Wang, X. Wang, A scalable chemical route to soluble acidified graphitic carbon nitride: an ideal precursor for isolated ultrathin g-C_3N_4 nanosheets, Nanoscale 7 (2015) 8701–8706.
[30] J. Zhang, M. Zhang, L. Lin, X. Wang, Sol processing of conjugated carbon nitride powders for thin-film fabrication, Angew. Chem. Int. Ed. Engl. 54 (2015) 6297–6301.
[31] Z. Zhou, J. Wang, J. Yu, Y. Shen, Y. Li, A. Liu, S. Liu, Y. Zhang, Dissolution and liquid crystals phase of 2D polymeric carbon nitride, J. Am. Chem. Soc. 137 (2015) 2179–2182.
[32] H. Yang, W. Zhenhai, C. Shumao, G. Xiaoru, C. Junhong, Constructing 2D porous graphitic C_3N_4 nanosheets/nitrogen-doped graphene/layered MoS_2 ternary nanojunction with enhanced photoelectrochemical activity, Adv. Mater. 25 (2013) 6291–6297.
[33] M.J. Bojdys, M. Jens-Oliver, A. Markus, T. Arne, Ionothermal synthesis of crystalline, condensed, graphitic carbon nitride, Chem.-Eur. J. 14 (2010) 8177–8182.
[34] J. Liu, T. Zhang, Z. Wang, G. Dawson, C. Wei, Simple pyrolysis of urea into graphitic carbon nitride with recyclable adsorption and photocatalytic activity, J. Mater. Chem. 21 (2011) 14398.
[35] Y. Dong, R. Wang, H. Li, J. Shao, Y. Chi, X. Lin, G. Chen, Polyamine-functionalized carbon quantum dots for chemical sensing, Carbon 50 (2012) 2810–2815.
[36] Y. Zhou, L. Zhang, W. Huang, Q. Kong, X. Fan, M. Wang, J. Shi, N-doped graphitic carbon-incorporated g-C_3N_4 for remarkably enhanced photocatalytic H_2 evolution under visible light, Carbon 99 (2016) 111–117.
[37] A. Thomas, A. Fischer, F. Goettmann, M. Antonietti, J.-O. Mueller, R. Schloegl, J.M. Carlsson, Graphitic carbon nitride materials: variation of structure and morphology and their use as metal-free catalysts, J. Mater. Chem. 18 (2008) 4893–4908.
[38] Z. Lin, X. Wang, Nanostructure engineering and doping of conjugated carbon nitride semiconductors for hydrogen photosynthesis, Angew. Chem. Int. Ed. Engl. 52 (2013) 1735–1738.
[39] X. Bai, L. Wang, R. Zong, Y. Zhu, Photocatalytic activity enhanced via g-C_3N_4 nanoplates to nanorods, J. Phys. Chem. C 117 (2013) 9952–9961.
[40] Y. Zeng, X. Liu, C. Liu, L. Wang, Y. Xia, S. Zhang, S. Luo, Y. Pei, Scalable one-step production of porous oxygen-doped g-C_3N_4 nanorods with effective electron separation for excellent visible-light photocatalytic activity, Appl. Catal. B-Environ. 224 (2018) 1–9.
[41] Y. Cui, Z. Ding, X. Fu, X. Wang, Construction of conjugated carbon nitride nanoarchitectures in solution at low temperatures for photoredox catalysis, Angew. Chem. Int. Ed. Engl. 124 (2012) 11984–11988.
[42] Y. Li, J. Zhang, Q. Wang, Y. Jin, D. Huang, Q. Cui, G. Zou, Nitrogen-rich carbon nitride hollow vessels: synthesis, characterization, and their properties, J. Phys. Chem. B 114 (2010) 9429–9434.
[43] A.B. Jorge, D.J. Martin, M.T.S. Dhanoa, A.S. Rahman, N. Makwana, J. Tang, A. Sella, F. Cora, S. Firth, J.A. Darr, P.F. McMillan, H_2 and O_2 evolution from water half-splitting reactions by graphitic carbon nitride materials, J. Phys. Chem. C 117 (2013) 7178–7185.
[44] P. Niu, L. Zhang, G. Liu, H.-M. Cheng, Graphene-like carbon nitride nanosheets for improved photocatalytic activities, Adv. Funct. Mater. 22 (2012) 4763–4770.
[45] Y. Huang, Y. Wang, Y. Bi, J. Jin, M.F. Ehsan, M. Fu, T. He, Preparation of 2D hydroxyl-rich carbon nitride nanosheets for photocatalytic reduction of CO_2, RSC Adv. 5 (2015) 33254–33261.
[46] Y.S. Jun, E.Z. Lee, X.C. Wang, W.H. Hong, G.D. Stucky, A. Thomas, From melamine-cyanuric acid supramolecular aggregates to carbon nitride hollow spheres, Adv. Funct. Mater. 23 (2013) 3661–3667.
[47] H.X. Li, Z.F. Bian, J. Zhu, D.Q. Zhang, G.S. Li, Y.N. Huo, H. Li, Y.F. Lu, Mesoporous titania spheres with tunable chamber stucture and enhanced photocatalytic activity, J. Am. Chem. Soc. 129 (2007) 8406–8407.
[48] J.S. Zhang, J.H. Sun, K. Maeda, K. Domen, P. Liu, M. Antonietti, X.Z. Fu, X.C. Wang, Sulfur-mediated synthesis of carbon nitride: band-gap engineering and improved functions for photocatalysis, Energy Environ. Sci. 4 (2011) 675–678.